Journal of Energy Storage 69 (2023) 107876

Contents lists available at ScienceDirect

Journal of Energy Storage

journal homepage: www.elsevier.com/locate/est

Research Papers

Experimentally based testing of the enthalpy-porosity method for the numerical simulation of phase change of paraffin-type PCMs

Arnold Martínez [a,b], Mauricio Carmona [a,*], Cristóbal Cortés [c], Inmaculada Arauzo [c]

[a] Rational Use of Energy and Environment Preservation Research Group from Universidad del Norte, Barranquilla, Atlántico, Colombia
[b] Engineering, Science and Technology - I.C.T Research group from Universidad de Córdoba, Montería, Córdoba, Colombia
[c] Department of Mechanical Engineering, University of Zaragoza, Campus Río Ebro. Building B. María de Luna s/n, 50018 Zaragoza, Spain

ARTICLE INFO

Keywords:
PCM
DSC
Numerical simulation
Properties determination
Unconstrained melting

ABSTRACT

The enthalpy-porosity method is generally applied as an economical resort for the numerical simulation of phase change materials (PCMs). However, having been developed strictly for metals, its suitability for the task is unclear, nor is the rationale for assigning its internal parameters, e.g., latent enthalpy and the constant of the momentum source term representing the "mushy" region. We first experimentally and exhaustively characterize a paraffin-type PCM, including differential scanning calorimetry (DSC) at several heating rates, T-history, and fusion visualization. Then, we develop a numerical model and systematically run simulations under different internal parameters and thermophysical properties of the PCM. Simulation results exhibit significant disagreement with experiments that cannot be reduced by any strategy for combining different material properties and model parameters. Among other effects, the constant of the momentum source term, which has to be assigned somewhat arbitrarily, has more relevance in the accuracy than any set of properties obtained by DSC and other experimental techniques. Thus, a rather negative, although interesting, conclusion is suggested: the enthalpy-porosity method may fail to model the phase change of paraffin-type PCMs. This is, of course, of paramount importance for the studies of their utilization in practical systems since it puts a fundamental point of uncertainty in any numerical study or lumped-type model derived thereof. The paper concludes with a tentative discussion of the possible causes of this failure and perspectives for developing more proper models.

1. Introduction

Interest in renewable energies has increased in recent years due to the future depletion of fossil fuel energy sources and the concerns about the effect of their use on climate change [1]. Solar energy is one of the areas of most significant development and highest energy generation potential. However, for low-temperature heating applications, although the cost of solar collectors for water and air has decreased due to technological improvements, its use in thermal applications is still low, mainly by the dispersion and intermittency of this energy source. In this context, energy storage is of paramount importance.

Using latent heat storage systems has advantages over sensible heat, so phase change materials (PCM) can have a significant role in developing solar thermal technologies, storing and releasing energy at an almost constant temperature linked with the phase change. For the successful use of PCM, a good experimental characterization of its thermal properties is required. Indeed, the thermal characterization of a material encompasses the properties needed for calculating energy storage, energy release, and space requirements, among others. Also, the detailed numerical modeling of processes involving PCMs, essential for proper design, benefits from an appropriate experimental characterization.

For this thermal characterization, a set of measurement standards must be followed. It happens that most of these standards were defined for other purposes or materials, so they do not fit the aim of thermal characterization, although they are used for this purpose [2]. For example, DSC is the most widely used method for the determination of thermal properties since it allows to estimate the characteristic temperatures (melting, crystallization, polymorphous transitions, reactions, glass transitions), the transformation and reaction heat (enthalpies), as well as decomposition, thermal stability, oxidation, and specific heat Cp.

Some standards applied to obtaining PCM properties using the DSC

* Corresponding author.
E-mail addresses: arnoldg@uninorte.edu.co, arnoldrafael@correo.unicordoba.edu.co (A. Martínez), mycarmona@uninorte.edu.co (M. Carmona), tdyfqdb@unizar.es (C. Cortés), iarauzo@unizar.es (I. Arauzo).

https://doi.org/10.1016/j.est.2023.107876
Received 27 February 2023; Received in revised form 11 May 2023; Accepted 29 May 2023
Available online 9 June 2023

are ASTM D87 [3] to determine the melting point of petroleum-derived waxes, ASTM D4419 [4] to determine transition temperatures, ASTM E793 [5], which is used to measure the enthalpies of fusion and crystallization through DSC, among others. This kind of standards, not designed for latent energy storage materials, also have been used to determine the properties of mixtures [6], composite materials [7,8], and porous matrices with PCM [9,10].

A drawback of DSC is that the mass of the sample and the rate of cooling/heating affect the experimental results [11]. Reference [12] proposes a methodology to avoid the variability of some parameters that influence the determination of the enthalpy curve as a function of temperature by DSC by using the dynamic method. Good fits were found for the heating tests; however, large deviations were observed in the cooling tests. A procedure to standardize the measurements, which includes recommendations for the calibration of the DSC equipment, as well as the selection of the cooling/heating rate, the measurement itself, and the way to analyze and present the data, is shown in [13]. Reference [14] suggested testing samples with a constant mass and a low heating speed to approximate thermal equilibrium. Reference [15] proposed a new method for DSC that considers the partially melted phases, being able to determine an endset temperature independent of the heating rate. However, the dependence persisted for the onset point. The German quality association RAL has also recommended varying the heating and cooling rates to minimize the differences between the heating/cooling curves [15,16].

The small sample sizes required for DSC measurements can cause material homogeneity issues, especially for mixtures such as paraffin waxes. A review of several devices built to assess thermal-physical properties, such as the measurement of diffusivity and thermal conductivity and enthalpy-temperature curves, is carried out by [17]. One of the methods developed for determining some thermophysical properties is the T-history method [18], later adjusted by [19] to obtain enthalpy-temperature curves. The T-history advantages are its relative simplicity and low cost and that, being a non-commercial device, it is possible to carry out a particular assembly according to the specific range of the application to be evaluated. On the other hand, when testing larger samples, crystallization is easier than with smaller samples, as those required by DSC. In particular, when testing PCMs with undercooling in a DSC, the maximum undercooling determined does not represent the PCM in an application [20]. DSC and T-history results are similar, with the advantage that the latter allows testing of non-homogeneous materials such as salt hydrates. Moreover, studies demonstrate this method's validity compared to DSC in materials such as paraffin waxes, salt hydrates, and fatty acids [21–24].

An adequate characterization of PCM is a requirement for numerical modeling. The most used approaches in the specialized literature since the 1970s are the effective heat capacity method and the enthalpy-porosity method. Although both are reasonably accurate, they also have inherent drawbacks. In the enthalpy method, handling supercooling and temperature swing problems is challenging. The effective heat capacity method must use a heat capacity curve determined at heating rates similar to the simulated experiment and ignores possible buoyant movement of the liquid, i.e., a purely diffusional problem is solved. It also has difficulties when the phase change temperature range is small, and it is not applicable for cases where the phase change occurs at a constant temperature [25].

A wide variety of heat transfer studies have been carried out in spherical and cylindrical containers. Reference [26] presents a numerical and experimental study of the RT27 commercial paraffin unrestricted movement melting process in a spherical container. Their numerical simulations considered a multiphase VOF model in which 85 % of the volume is initially filled with PCM on a two-dimensional axisymmetric domain. They used the enthalpy-porosity method with a value of the mushy zone constant C of 10^5. The thermophysical properties were those provided by the manufacturer; however, the article does not account for the determination of the variable values of the properties used, i.e., the thermal conductivity and specific heat, as well as the determination of the viscosity or the variation of density.

In reference [27], experimental research on the melting process of n-octadecane using two approaches is presented: restricted movement (the PCM is prevented from sinking to the bottom of the container because the material remains attached to the thermocouples) and unrestricted movement (there are no thermocouples, so the solid PCM sinks due to gravitation). The experimental results were compared with the numerical ones to understand the role of buoyancy-induced convection during restricted and unrestricted fusion within the spherical capsule. The thermophysical properties of the material were considered constant in both phases, using the Boussinesq approximation for modeling free convection. Results showed a fair agreement in the liquid fraction. There were, however, deviations in the thermocouple readings, which were believed to be caused by thermal stratification inside the bath in which the sample was dipped. A phenomenon related to the fusion of PCMs is the existence of simultaneous layers of thermally stable and unstable fluid along the axis of symmetry, discussed in reference [28]. At the top, the fluid layers are stratified horizontally, with the denser fluid below the lighter hot layers. At the bottom of the container, the axis of symmetry features recirculation cells that generate a hot column of liquid rising toward the bottom surface of the remaining solid PCM, which is corrugated as a result.

In reference [29], an experimental rig is developed to measure the temperatures inside a cylindrical container filled with PCM (n-eicoisane). The melting front during the heating of the PCM is graphically reported so that the results are used as a reference for the validation of numerical codes. They compared the results with a computational model using the enthalpy-porosity method. The thermophysical properties of n-eicoisane were obtained from other references in the specialized literature and were assumed to be constant with temperature except for viscosity. Comparisons between the experimental measurements and the numerical predictions for the melt front locations and the temperature data revealed reasonable overall agreement for Stefan numbers up to 0.1807. Reference [30] develops numerical and experimental research of the melting process in a vertical cylindrical container filled with commercial RT27 paraffin whose melting interval was 26–28 °C. The VOF method was used to simulate the expansion of the PCM when melting, generating an interface between the PCM and air without interpenetration. The thermophysical properties were those indicated by the manufacturer, and dynamic viscosity was adjusted with a third-degree polynomial. In this study, the effects of the mushy zone constant, the pressure-velocity coupling, and the pressure discretization schemes on the thermal behavior of the fusion process were analyzed. A quantitative agreement was obtained between the simulations and the experiments. However, this reference does not consider the variation of thermophysical properties with temperature, except for thermal conductivity, which is modified to achieve more realistic results, without indicating how the new property values were obtained. The authors suggest using $C = 10^8$, considering the results for two different temperature excesses ΔT. Still, it was not verified if this value would be recommended for a cylinder of different dimensions.

In reference [31], a numerical study of the fusion and solidification processes inside a spherical container of n-octadecane using constant and variable thermophysical properties is presented. They used the enthalpy-porosity model and compared the results in 2 and 3 dimensions with those obtained numerically by [28]. The authors compiled the thermophysical properties of PCM from different sources. They find difficulties because there are few references in the literature of these properties at temperatures close to the phase change, especially density values in the solid phase, thermal conductivity of both phases and melting temperature. Moreover, there were significant discrepancies between the different sources in some cases. For instance, [32] found that impurities could modify the behavior of pure compounds such as n-octadecane, resulting in changes in the melting temperature and latent heat of fusion. These behavior changes can also occur by adding some

materials to improve the thermal properties [33,34]. The models evaluated by [31] considered a convection coefficient between the spherical cover and the water bath to avoid the stratification problems mentioned by [28]. They tested two values: one of them considering a high heat transfer rate between the water bath and the capsule and the other with a low heat transfer rate. However, the assumption of the values of the heat transfer coefficients became an additional source of discrepancies in the results obtained. The authors also considered a linear variation between the density and specific heat values in each phase, finding that the simulations were 8 % slower, assuming an increase in the latent heat of fusion according to the relationship between solid and liquid densities (ρ_s/ρ_l). It was found that this increase compensates for the change in properties between both phases, finding that the expansion in the fusion process is not very significant for this case. The simulations showed that the 3D model could reproduce flow patterns in the unstable thermal zone that cannot be simulated with a two-dimensional treatment. However, the global liquid fraction evolution does not appear to differ significantly between the 2D and 3D simulations.

In reference [35], a critical review of the melting and solidification process inside a spherical capsule is carried out. They found that most studies were conducted at a fixed temperature, the simplest case describing the external thermal conditions. This approach does not guarantee an accurate calculation of practical heat transfer characteristics for the available PCMs. Due to the lack of exhaustive and systematic experimental studies of heat transfer during the melting and solidification process, the authors suggested that future research be oriented in three main fields:

(i) The thermophysical properties should be measured reliably, including melting point, heat of fusion, thermal conductivity, density, specific heat in the solid and liquid state, as well as the viscosity in the temperature region near the melting point.
(ii) When investigating mixtures, their properties, particularly viscosity, must also be accurately measured since an incorrect parameter value can contribute significantly to a deviation of the numerical results from the experimental data.
(iii) The presentation of the results in graphical and tabular form is recommended, as well as the production of the results in dimensionless form.

One of the main challenges in PCM numerical simulation is dealing with density values during the phase change. Most models described in the literature consider the Boussinesq approximation to model the effects of natural convection in the liquid phase. That is, density is deemed constant except in the buoyancy term of the momentum equation, where its difference with a reference value is considered proportional to temperature difference. This neglects the volumetric variation of the PCM on fusing, which could be between −8.3 % and 22 % [36].

The variability of properties with the rate of heating/cooling in DSC has also been studied in several works. In reference [37], the Cp-T relationships at heating rates of 10 °C/min and heating/cooling rates of 0.2 °C/min are experimentally determined. They modeled the system by comparing both curves of the effective heat capacity, finding that the error in the determination of the PCM temperature in the numerical model decreased from 10.5 % to 3.5 % for the lowest speed and from 19.5 % to 3.0 % concerning the experimental results, for the unloading and loading processes respectively.

Reference [38] evaluates experimentally and numerically a wall with PCM to provide data for the validation of building energy performance simulation tools. For this study, three Cp curves obtained by DSC under different experimental conditions were considered to evaluate the effects of the complete and incomplete phase transition and the modeling of hysteresis in the material. It was found that more advanced modeling of the phase change allows the results to be consistent with the thermophysical phenomena of the composite PCM under actual conditions and achieves more reliable results.

More recent works on this matter are related to the phase change phenomenon under different container configurations. In [39], a numerical analysis of PCM melting with internal/external fins serves to study the effect of varying fin designs on the phase change behavior. Similar work is presented in [40], where differently shaped containers are considered in the melting process of different PCMs. Other works, such as [41], evaluate using different PCMs inside the same container, but in separated chambers. Various geometrical configurations are proposed and evaluated by numerical simulation.

It is difficult to find a consensus for modeling applications of latent energy storage, mainly due to the physicochemical characteristics of the materials and the lack of a specific standard for the measurement of properties. The literature review above indicates that the research on the fusion of PCMs is approached considering approximately constant properties, or only some of them variable with temperature. In addition, the numerical models consulted scarcely consider that the heat rate at which calorimetry is performed directly affects the values of the properties being measured. Despite the variability of the results in determining properties, the enthalpy-porosity method seems to fit in each case. However, the lack of agreement in liquid fraction curves and fusion fronts is noticeable, even for cases with a low average difference.

This research seeks to contribute to the question by systematically investigating how the values of thermophysical properties determined by calorimetry (DSC) must be used in the numerical model of the melting process of a paraffin-type PCM in cylindrical containers through the enthalpy-porosity method. In addition, results considering a variable density and the ensuing expansion, modeled by the volume-of-fluid (VOF) method, are compared with those assuming the Boussinesq approximation to determine if the simplification is justified concerning computational savings. Finally, scenarios with different values of the constant of the mushy region are evaluated to ascertain its role in the numerical modeling of the process. This kind of systematic study has not been reported previously in the literature, where apparently blind confidence in the enthalpy-porosity method dominates many investigations.

The research uses experimental values by DSC, T-history, and other determinations of properties, to compare measurements collected during fusion visualization tests with the results of their numerical simulation employing the implementation of the enthalpy-porosity method included within the framework of the CFD methods of the Fluent code 2020 R2 [42]. Results indicate that there is no simple rationale to assure good agreement with experiment under all circumstances. Moreover, the constant of the mushy region has a determining influence, and it is not possible to develop indications for a proper selection, which seems situation-dependent.

The paper concludes by preliminarily discussing possible factors that contribute to this lack of accuracy of the enthalpy-porosity method, the consequences for the computation of practical systems, and the possible approaches to developing more accurate models.

2. Experimental work

2.1. Determination of thermophysical properties by differential scanning calorimetry

For the experimental work, the commercial paraffin RT45 distributed by Rubitherm Technologies GmbH was used, which has a declared temperature range for melting between 41 °C and 46 °C. The DSC technique was used to determine the latent heat of fusion, the start and end temperatures of the phase change, as well as the values of the specific heats. Unlike a pure material where the phase change occurs at a constant temperature, commercially available PCMs for thermal energy storage applications are manufactured from mixtures of different compounds, and the fusion develops over a range of temperatures. To carry out the calorimetry, the DSC 250 equipment (TA Instruments) of the Discovery series was used, with an RCS90 refrigeration system which

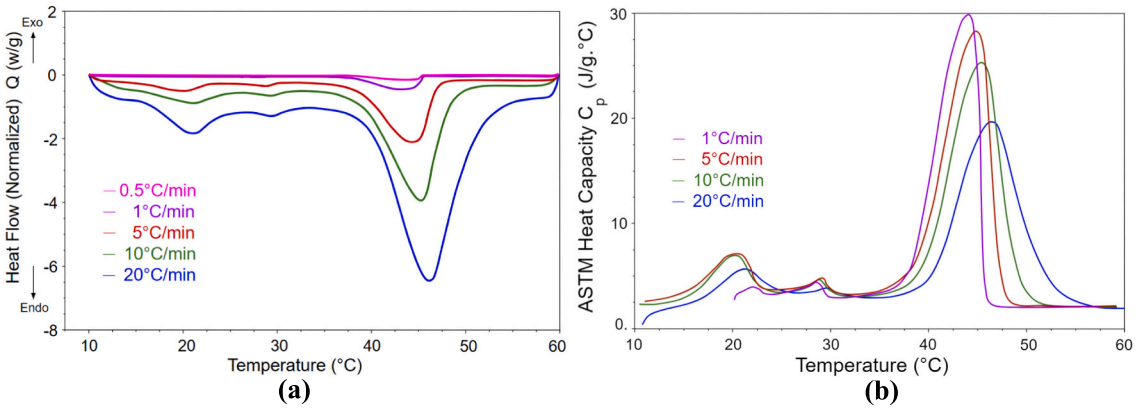

Fig. 1. DSC results for different heating rates. a) Heat flow b) ASTM heat capacity.

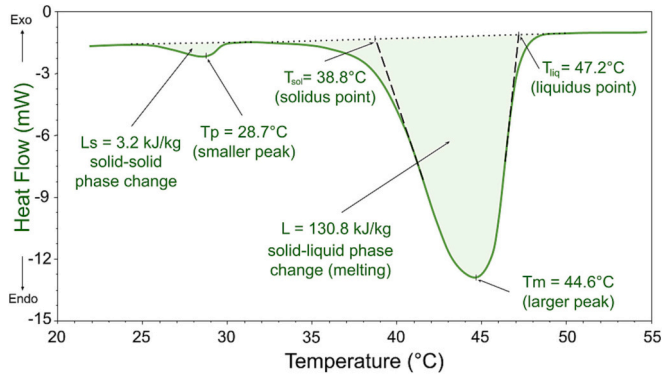

Fig. 2. DSC thermogram obtained at a heating rate of 5 °C/min.

allows tests to be carried out in a range between −90 °C and 550 °C. The experiments were conducted with 5 to 6 mg of RT45 under Nitrogen (N_2) atmosphere with a flow rate of 50 ml/min. The DSC 250 works in a temperature range from −180 °C, with an accuracy of ±0.05 °C and a temperature precision of ±0.008 °C.

DSC determines the amount of heat a sample absorbs when the temperature varies. The temperatures in both the sample and the reference are monitored during the process. A temperature difference is used to determine the heat flux between the sample and the oven [43].

The determination of thermophysical properties in PCMs presents some difficulties from the experimental point of view, since they can present subcooling, hysteresis, and crystallization, all of which make it difficult to interpret the values determined. For calorimetry, there is the problem of the small size of the samples that are examined, and differences between the results may appear due to poor homogeneity of the material. Additionally, the results could vary when considering different heating or cooling speeds during the tests. The experimental determination of the thermophysical properties was carried out based on the ASTM D4419 standard [4]. For this, heating rates of 20, 10, 5, 1, and 0.5 °C/min were used: the procedure is described in more detail in [44]. For the tests, the samples of the sealed material were placed inside a crucible next to an empty reference crucible, which was simultaneously subjected to a temperature program at a given heating rate. At the same time, the difference in heat flow between the two was monitored. For the determination of the specific heat, the procedure indicated in the ASTM E 1269 standard was used [45]. Fig. 1(a) shows the experimental results obtained. Variation of the heat flow with the heating rate is observed, which generates a shift in the peak of the transition, as well as in the initial and final values of the phase change. The heat flow could be

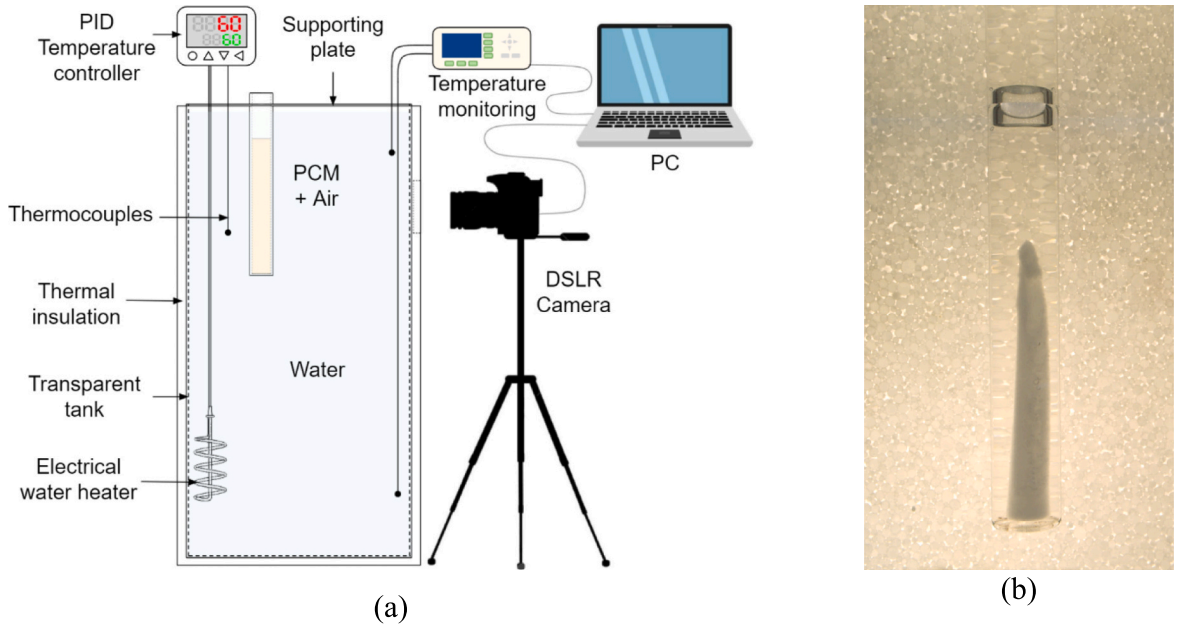

Fig. 3. (a) PCM fusion experimental set-up. (b) Identification of liquid and solid areas by photography.

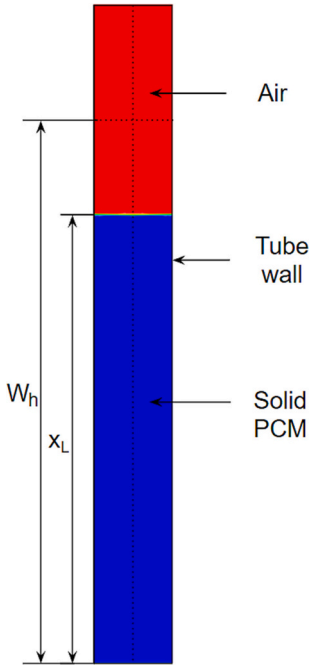

Fig. 4. Numerical model at t = 0.

normalized by dividing by the respective sample mass of each experiment. Fig. 1(b) shows the specific heat computed with the heat flow and the temporal variation of sample temperature. Two solid-phase transformations are observed before fusion occurs. For the lower heating rates, it is observed that the peak of specific heat becomes larger and larger, approaching the condition of thermodynamic equilibrium. There is also evidence of a slight shift of the curves to the left.

The points to determine the beginning and end of the phase change, the enthalpy, and the phase change temperature, are described in an example DSC thermogram, Fig. 2, obtained at a heating rate of 5 °C/min. In it, two peaks can be seen during heating: a smaller peak that corresponds to a solid-solid phase change at a temperature of 28.7 °C and a higher peak at 44.6 °C, which is the melting point of the material at this rate, at which the phase change from solid to liquid occurs. The value of the beginning of the phase change can be identified, defined as the intersection between the tangent to the maximum upward slope of the peak and the baseline of the extrapolated sample. The end of the phase change can be obtained in an analogous way. The latent heat of fusion L (kJ/kg) is computed from the integration along time of the heat flow curves, from the start to the end of the main peak.

2.2. PCM fusion experiments in cylindrical containers

Fig. 3 shows a diagram of the experimental set-up developed for capturing the molten fraction inside the PCM and its evolution. The assembly consisted of a water tank, a glass test tube, temperature gauges (type K thermocouples), a thermal bath, PID control for the electric heater, and an 8-channel data acquisition system. The water was kept at a uniform temperature during the experiments by constant stirring (electric stirrer not shown). Three different temperatures were used inside the tank with water, 50, 55, and 60 °C. Once the uniform temperature of the test in the tank is reached, the cylindrical container partially filled with solid PCM RT45 is introduced to a determined volume.

The fusion profile tracking was made employing a DSLR Nikon D5200 camera, taking photographs every 5 s from the immersion of the sample in the thermal bath. Artificial lighting was placed on the back of the assembly to obtain a better contrast in the photographs. The solid area is easily distinguishable from liquid, being the latter transparent, as shown in Fig. 3(b). The molten fraction inside the sample was calculated with commercial CAD software, determining the proportion of the solid profile area of the sample with respect to the total sample area occupied by the PCM.

3. Numerical modeling

3.1. Physical model and numerical solution

A numerical model of the melting process was developed for a vertical test tube of 3 cm diameter filled with solid PCM without restriction of movement during the process, with an excess temperature ΔT of the water bath of 5, 10, and 15 °C above melting. 2-D axisymmetric behavior was assumed. A sketch is shown in Fig. 4. The length x_L is the height to which the tube is filled with solid PCM, and W_h is the level that the specimen was immersed to in the thermal bath. In the model, a uniform boundary temperature equal to that of the bath is considered up to the W_h level as well as at the bottom of the test tube. The lateral wall above W_h was at room temperature (27 °C), while the upper part of the domain was open to the atmosphere (pressure-outlet boundary condition) with an outside temperature of 27 °C. For our experiments, x_L = 0.16 m and W_h = 0.2 m (Total height = 0.235 m).

The enthalpy-porosity method was used together with the volume-of-fluid (VOF) approach considering the liquid and solid phases within the domain, separated by an interface with air initially located at the level x_L [46]. This approach allows the increase in volume as the PCM melts. The air was modeled assuming a density-temperature relation for air: $\rho = 1.2 \times 10^{-5}\,T^2 - 0.01134\,T + 3.4978$.

Two approaches for density are considered: (i) a linear variation in the mushy region from 880 kg/m^3 at T_s to 770 kg/m^3 at T_l. (ii) the Boussinesq approximation for the liquid phase, in which the density varies only considering the buoyancy term in the momentum equation, thus: $\rho = \rho_0(1 - \beta\,\Delta T)$, where ρ_0 is the reference density in the liquid phase, and β is the thermal volumetric expansion coefficient. The density in liquid and solid phases is considered constant, with 770 kg/m^3 and 880 kg/m^3, respectively. The initial temperature of the whole domain is 27 °C.

The enthalpy-porosity method has been widely used to model the melting/solidification process inside PCM containers where natural convection is significant. Representing the real physics demands to track the variable phase interface, coupled with the calculation of energy balances and temperature. This is extremely costly in terms of computational resources, so an artificial fixed-grid method is used. In a fusion/solidification problem for a fixed domain, the momentum equation has to be modified to consider the transition between the liquid and solid phases, guaranteeing that the velocities are zero in the latter. The main method to achieve this is to introduce a source term (S_u) of a great magnitude into the momentum equation:

$$\frac{\partial}{\partial t}(\rho u_i) + \frac{\partial}{\partial x_j}(\rho u_j u_i) = -\frac{\partial p}{\partial x_i} + \mu \frac{\partial^2 u_i}{\partial x_j \partial x_j} + \rho g_i + S_u \tag{1}$$

where ρ is density, and μ is dynamic viscosity. The term S_u modifies the moment balance depending on the phase. It varies from a high value imposing complete rest on the solid region, to a limit value of zero when the material becomes completely liquid. Moreover, this method was developed for alloys, wherein a two-phase liquid-solid region of intermediate composition appears. When dealing with the model of a 2D or 3D geometry, it is referred to as the "mushy" region, and determining its position/shape forms a part of the numerical problem.

Within this context, the source term of Eq. (1) is defined as

$$S_u = -A(\gamma)u_i \tag{2}$$

Here, A (γ) is the porosity function defined by Brent [47], which allows the moment equation to mimic the behavior of the flow in the mushy region of the PCM, defined by the Carman-Kozeny equation

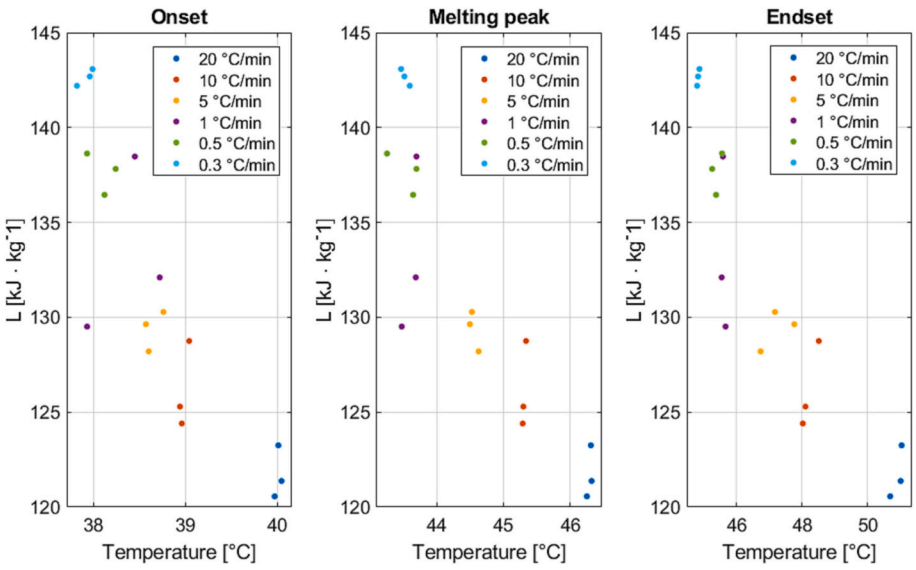

Fig. 5. Variation of the temperatures of start, end, and phase change for different heating rates.

derived from Darcy's law for a porous medium [22]:

$$A(\gamma) = \frac{C(1-\gamma)^2}{\gamma^3 + q} \tag{3}$$

where γ is the liquid volume fraction and C is the constant of the mushy zone, which depends on its morphology; large values make the damping of velocity stronger and thus a thin mushy region, approaching the situation of a pure substance. Values between 10^4 and 10^7 are recommended for most applications, although no well-based and general recommendations have been given for PCMs, whose phase behavior is presumably different from that of alloys. The constant q (0.001) is introduced to prevent division by zero. For the energy balance as a function of the liquid fraction and other details of this model, see Voller [48].

In order to introduce the dependence of liquid viscosity on temperature, the property was determined using a Hoppler viscometer, for which four measurements were made at 46, 50, 55, and 60 °C. A regression of the average results was determined and used in the model:

$$\mu_l = 2.283 \times 10^{-7}\, T^3 - 3.501 \times 10^{-5}\, T^2 + 0.001734\, T - 0.02587 \tag{4}$$

The numerical model based on the enthalpy-porosity method available in the ANSYS Fluent 2020 R2 code is used. For the spatial discretization of the model with 3 cm diameter, a structured mesh of 12,880 elements was chosen, while for the model with 2.2 cm diameter, a mesh of 6820 elements was chosen, which were selected after a study of grid convergence that will be discussed in the results section. For the spatial discretization of the equations, the Quick scheme was used to solve the momentum equation; the compressive scheme was adopted for the volume fraction and the Quick scheme for the energy equation. The PRESTO! scheme is used for pressure, coupled with velocity using the SIMPLE algorithm. A bounded, second-order implicit formulation was used for the transient calculation, and a constant time step size of 0.03 s was considered, with which independence in the results was achieved and was applicable in most cases without convergence problems [46]. This set of modeling choices follows the recommendations of [30].

All surfaces of the domain seen in Fig. 4 are assumed to obey the non-slip condition for fluid flow, except the top one, where an exit condition on pressure is specified, which allows air flow in both directions (only in the case of the VOF model). At $t = 0$, the solid PCM and the air are at room temperature, and the base and the lateral surface of the test tube up to immersion height W_h are put at the water temperature. A wall thickness model considers the conduction in the glass (thickness of 0.002 m). Ambient temperature is imposed on the lateral surface between W_h and the top of the tube.

During the calculation, the interface between the PCM and the air was tracked using the VOF method with an explicit formulation without phase interactions. The mushy zone was tracked using the enthalpy-porosity method between T_s and T_l. The formulation assumes that in the mushy region, the porosity is equal to the liquid fraction of the cell and that the fluid and solid velocities are equal in that region. Also, that the liquid fraction varies linearly with temperature [49]:

$$\gamma = \frac{T - T_s}{T_l - T_s} \tag{5}$$

Table 1
Thermophysical properties used for the numerical models.

Case	1	2	3	4	5	6	7
Heating rate [°C/min]	**n.a.**	**20**	**10**	**5**	**1**	**0.5**	**T-history**
T_s [°C]	41	40.0	39.0	38.6	38.4	38.2	37
T_l [°C]	46	50.9	50.9	46.9	45.6	45.4	47
T_m (main peak) [°C]	44	46.3	43.6	44.6	43.6	43.5	45
L [kJ/kg]	160	121.73	126.14	129.56	133.37	137.63	164.45
Cp,s [kJ/kg·K]	2	3.4	3.4	3.4	3.4	3.4	4.35
Cp.l [kJ/kg·K]	2	2.2	2.2	2.2	2.2	2.2	2.22
k_l [W/m•K]	0.2	0.156	0.156	0.156	0.156	0.156	0.156
k_s [W/m•K]	0.2	0.234	0.234	0.234	0.234	0.234	0.234

Case: Case studied Heating rate [°C/min]: the velocity of the heating for the tests n.a.: n.a.: not available (case 1 with manufacturer data) T-history: Experimental technique T-history.

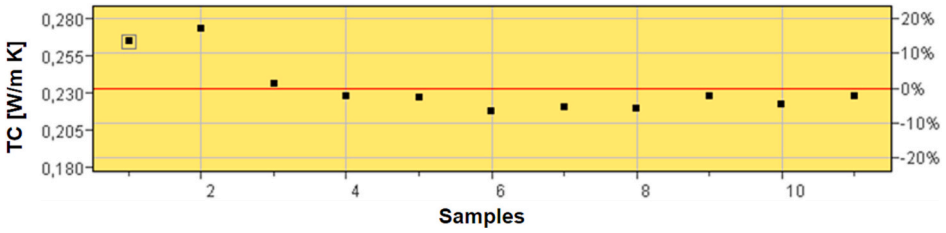

Fig. 6. Experimental measurement of PCM thermal conductivity in solid state.

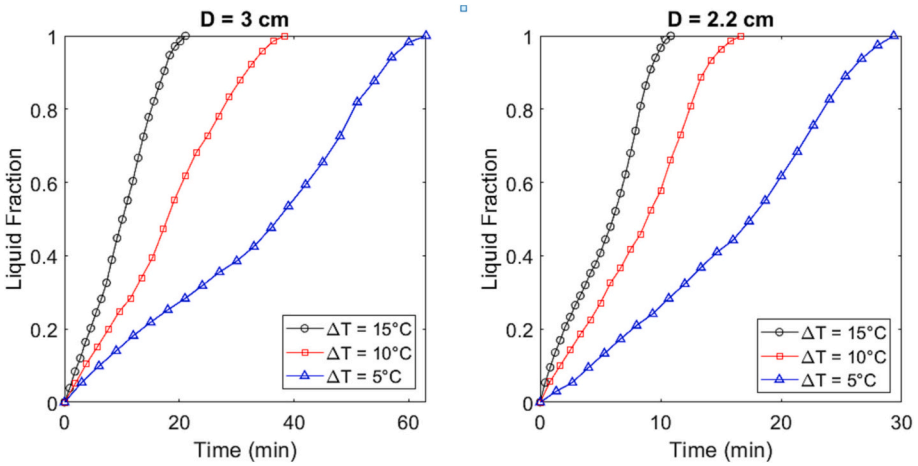

Fig. 7. Measured liquid fraction vs. time for different excess temperatures ΔT of the bath and test tube diameters.

4. Results

4.1. Experimental results

For the thermophysical properties measured by calorimetry, the strategy was to carry out five tests at heating rates of 0.5, 1, 5, 10, and 20 °C/min and average the results obtained for each of three repetitions of the tests. Fig. 5 presents the variations in the measurements of the start, end, and transition temperatures obtained by DSC with respect to the latent heat of fusion (*L*). The standard deviation of the solidus temperature (T_s) values for the measurements of 0.5, 1, 5, 10, and 20 °C/min were 0.06, 0.4, 0.1, 0.05, and 0.04, respectively. In the same way, for the end (T_l) of the phase change, standard deviations of 0.15, 0.06, 0.25, 0.26 and 0,19 were obtained. The different experimental measurements for the same heating rate seem quite consistent. The average values obtained for each property are presented in Table 1. For the heat of fusion, standard deviations of 1.1, 4.6, 1.3, 2.3, and 1.4 were obtained for the heating rates mentioned above, respectively.

The calorimetric measurements on the PCM were made using an average of 6 mg of sample. Global results are summarized in Table 1, which provides additionally the values given by the manufacturer. Additionally, the values of the properties obtained using the T-history method, as described in [44], were used in the computation.

In order to ascertain the thermal conductivity of the PCM, an experimental evaluation of the property was carried out following the procedure indicated in the ASTM D5334-08 standard, for which the TK04 equipment was used, whose precision is 2 %. The principle of measurement is based on introducing a needle probe into the sample, which is subsequently heated with a constant power while recording the temperature increase over time within the source. To counteract the effects associated with the poor homogeneity of the material, 11 measurements were made in solid state at 27 °C (see Fig. 6), with an average value of 0.234 W/m•K. Tests were carried out varying the temperature above the phase change temperature by means of a thermal bath, in order to obtain the thermal conductivity in the liquid state; however, it was difficult to achieve thermal equilibrium except in one of the tests at 58 °C, for which the value resulted in 0.156 W/m•K.

For the numerical models, the thermal properties indicated in Table 1 were used, as well as the values of the viscosity and thermal conductivity obtained experimentally. In the case of the data supplied by the manufacturer, a constant value of 0.2 W/m•K is considered for thermal conductivity in both phases. In the case of T-history, the data obtained in the conductivity tests are used. For the measurement of the T-history, special-class type K thermocouples with an accuracy of ±0.1 °C were used.

Results for liquid fraction evolution during the fusion of the PCM RT45 are shown in Fig. 7. A similar pattern can be observed for each ΔT between the two sizes; however, the melting time for the larger test tube is doubled compared to the smaller test tube.

Evolution of the fusion contours obtained experimentally for the test tube with a diameter of 3 cm is shown in Fig. 8, representing the unitary solid fraction contours measured over time. The graph shows that the physics is not entirely axisymmetric, surely influenced by convective currents of the liquid within the sample.

As it is evident, for a smaller temperature difference between the wall and the sample, the process takes longer. In general terms, the same pattern of evolution with time is observed for all the experiments.

4.2. Numerical results

This section compares the numerical results obtained using different thermophysical properties of the PCM, as detailed in Table 1, while it is subjected to a fusion process inside a test tube. For this, different mesh sizes were considered for testing numerical error and grid independence. Fig. 9 shows the results for the test tube of 3 cm diameter. A growing number of elements was tested, 3290, 6720, 12,880, and 26,840. Numerical results of the molten fraction and a virtual thermocouple located in the middle axis at 6 cm from the base of the test tube are plotted.

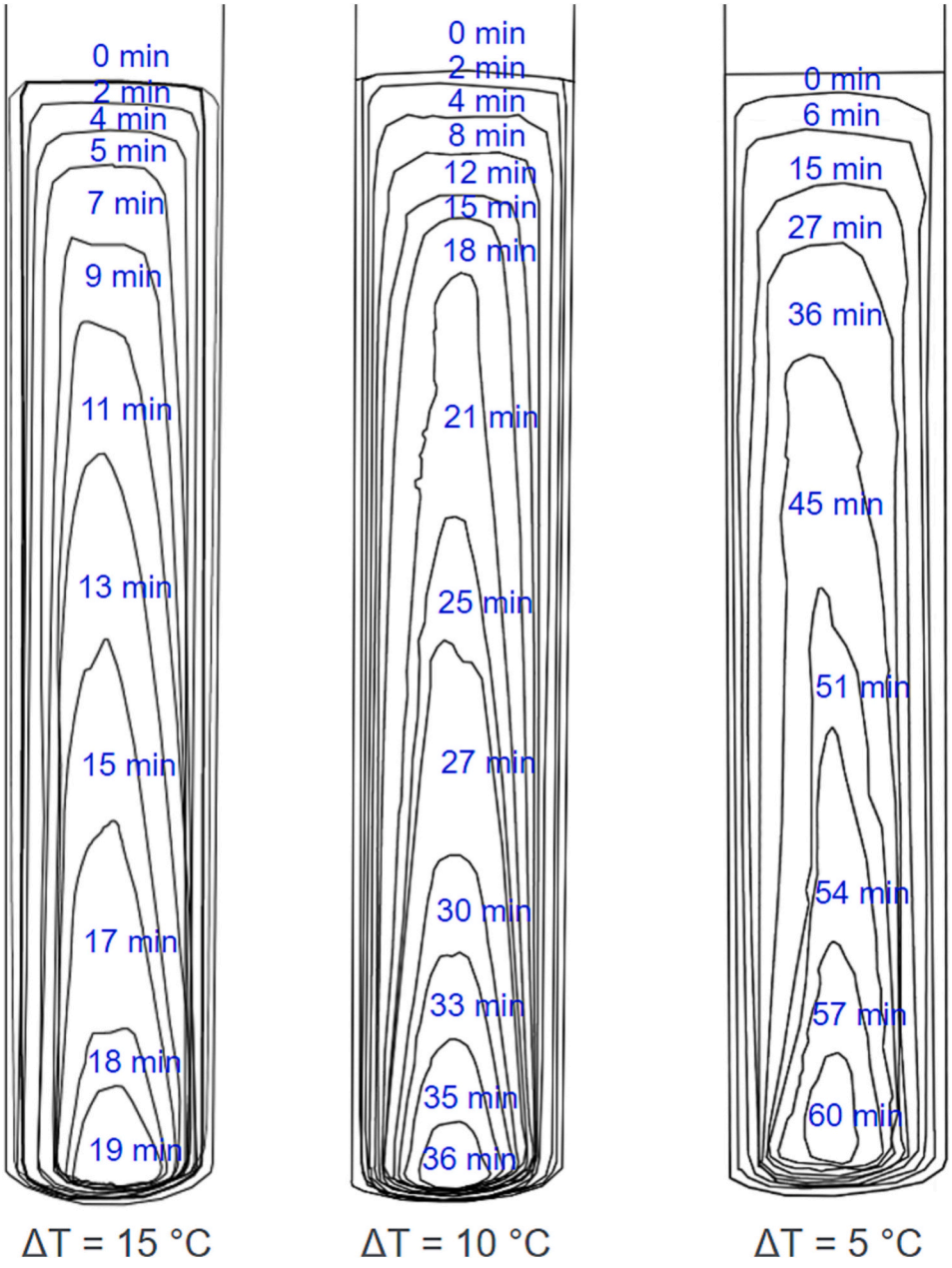

Fig. 8. Graphical evolution of the fusion contours according to excess temperature in the walls.

Results show significant discrepancies and chaotic behavior in PCM temperature in the case of 3290 elements, whereas all results stabilize for progressively denser grids. Consequently, intermediate values of 6720 and 12,880 elements were chosen for the numerical computations with diameters of 2.2 and 3 cm.

The numerical results show that the constant C of the mushy zone plays a determining role in the experimental agreement of the numerical predictions. Fig. 10 shows an example for the test tube of diameter 2.2 cm. It indicates that, as the constant value is increased, the melting of the PCM is delayed. It is also evident that special care is needed in selecting its value. With proper adjustment, total fusion time can be predicted. However, the evolution of the liquid fraction can be only approximated, with no ability whatsoever to predict the observed changes in temporal slope. Further details on C value selection are discussed below.

Fig. 11 shows the results for the melted fraction using $C = 10^6$ for the case $\Delta T = 15$ °C. Those obtained considering a variable density agree better in general terms with the experimental results than those obtained using the Boussinesq approximation. However, the latter is found to mimic very well the experimental results with the T-history values of the properties and those at a heating rate of 20 °C/min.

Fig. 12(a) shows the results for ΔT equal to 10 °C in which a constant C of 10^7 was considered, while Fig. 12(b) shows some results for ΔT equal to 5 °C with a constant C of 10^7 and 10^8, since the discrepancies with the experimental results were greater if a single value for C was used.

Fig. 12(a and b) compares numerical and experimental liquid fraction results for the case of $\Delta T = 10$ °C. The results vary in a wide range, predicting that the fusion occurs 27 % before or after the experimental time in some cases. In this case, it is also observed that none of the numerical curves for a ΔT of 10 °C fits as well as for the case $\Delta T = 15$ °C. The curves that presented the best fit in this case were those with the properties obtained with 10, 5, and 0.5 °C/min with variable density and, in the case of T-history, with the Boussinesq density. It is also possible to show that they fit better for the simulated data set when C =

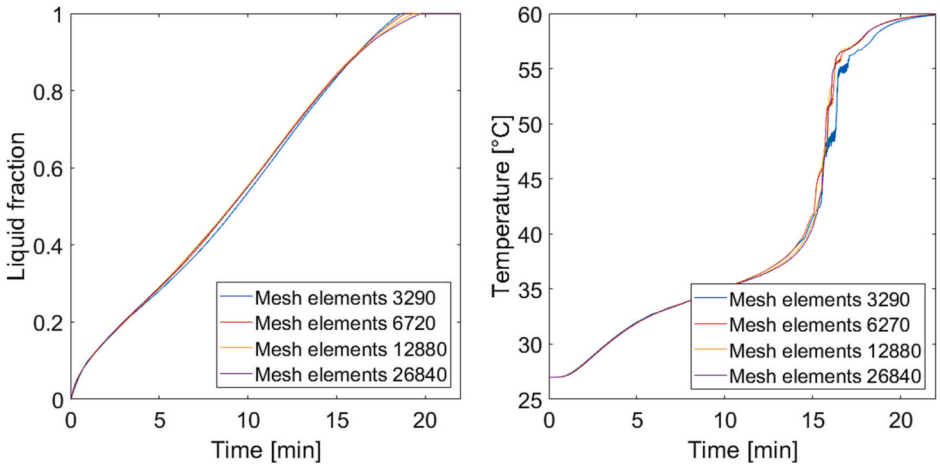

Fig. 9. Numerical results of grid independency for fused fraction (left) and PCM inner temperature (right).

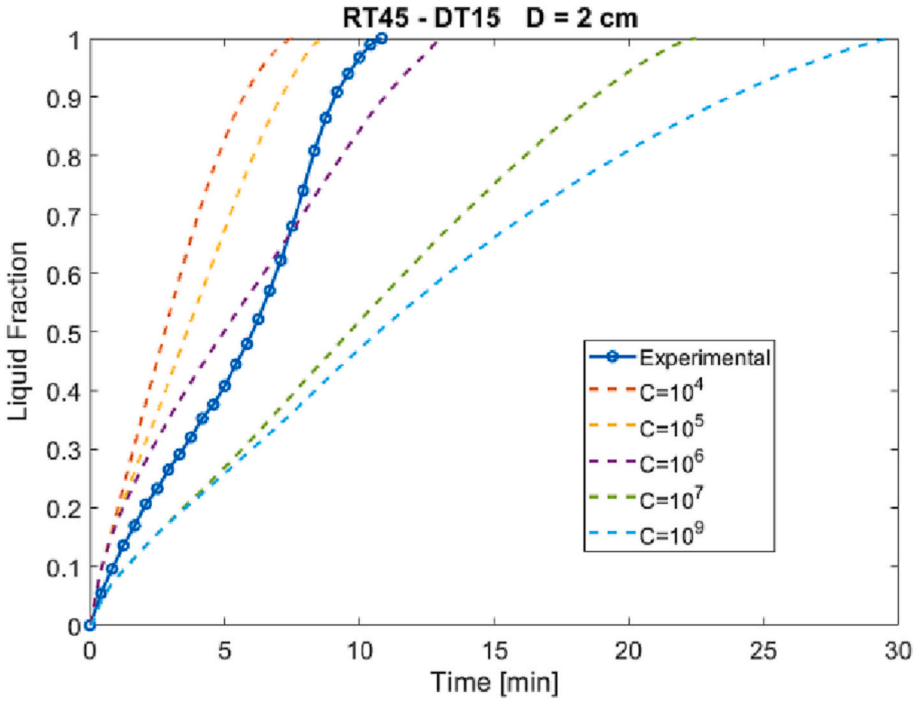

Fig. 10. Effect of the parameter *C* in the numerical model.

10^7 (b) is used instead of C = 10^6 (a).

The case with a ΔT of 5 °C of Fig. 12(c and d) shows that the numerical results do not agree with the experimental data so well, although in some cases, the start and end of the phase change are close. This case of the slower melting studied makes it evident that the numerical results cannot predict the variations of the curvature exhibited by the experimental curve.

In order to compare the experimental fusion profiles with the numerical ones, the cases with the best fit for each excess temperature were selected. Figs. 13, 14, and 15 present graphically the evolution of the molten fraction of the PCM in the test tube with a diameter of 3 cm. For each ΔT, the results of the 4 cases that best fit the experimental data are shown. The first moments of fusion in each case exhibit a realistic behavior, as well as the upper part of the fusion front. However, formation of dendrites is appreciated in the lower part of the solid PCM. This is the same numerical artifact observed in [28,31], due to the simplification of the boundary condition as a uniform wall temperature for representing the external heating. In this case, the magnitude is more appreciable, perhaps because an isothermal angled boundary will artificially induce a very large heat flux at the corner, at least during the first instants, when diffusion dominates. As studied in [31], it is intricate to solve this question via simple expedients, such as a uniform convective coefficient. A more accurate representation is needed, which would be indeed very difficult for a stirred water bath.

On the other hand, the formation of dendrites is also strongly influenced by the constant C, as seen in Fig. 16, which shows the evolution of the fusion contours for a diameter of 2.2 cm, varying *C* from 10^4 to 10^8. In order to reduce the variability in the results shown, the same data set was considered for the thermal properties obtained at a heating rate of 20 °C/min and variable viscosity for all models. It is observed that with a value of 10^4, it presents the most realistic contours. However, in this case, the numerical fusion occurs much faster than in reality, as evidenced in Fig. 10. Starting from C = 10^5, the formation of dendrites appears, increases up to C = 10^6, and then decreases as the value of the constant is increased. However, when increasing C beyond 10^8, no significant variation is observed in the curves and fusion contours,

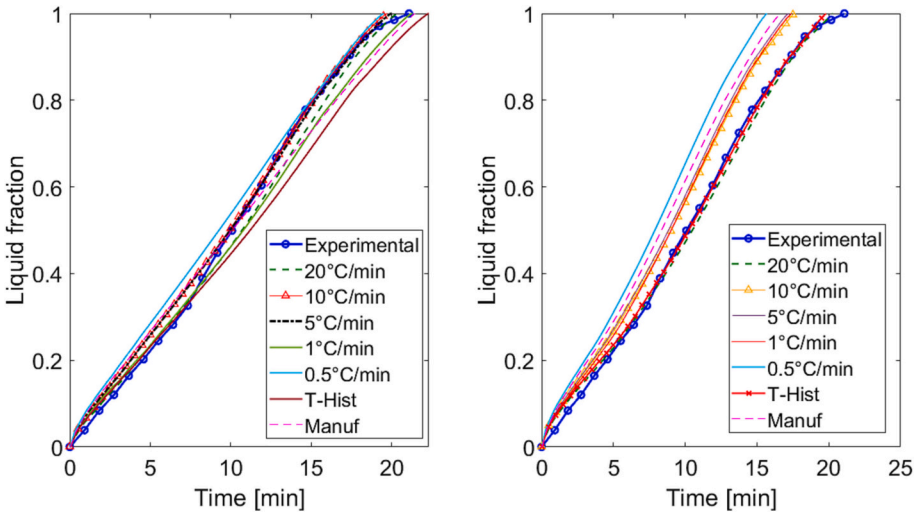

Fig. 11. Numerical results with C = 10^6 for different cases, assuming a) variable density b) Boussinesq approximation.

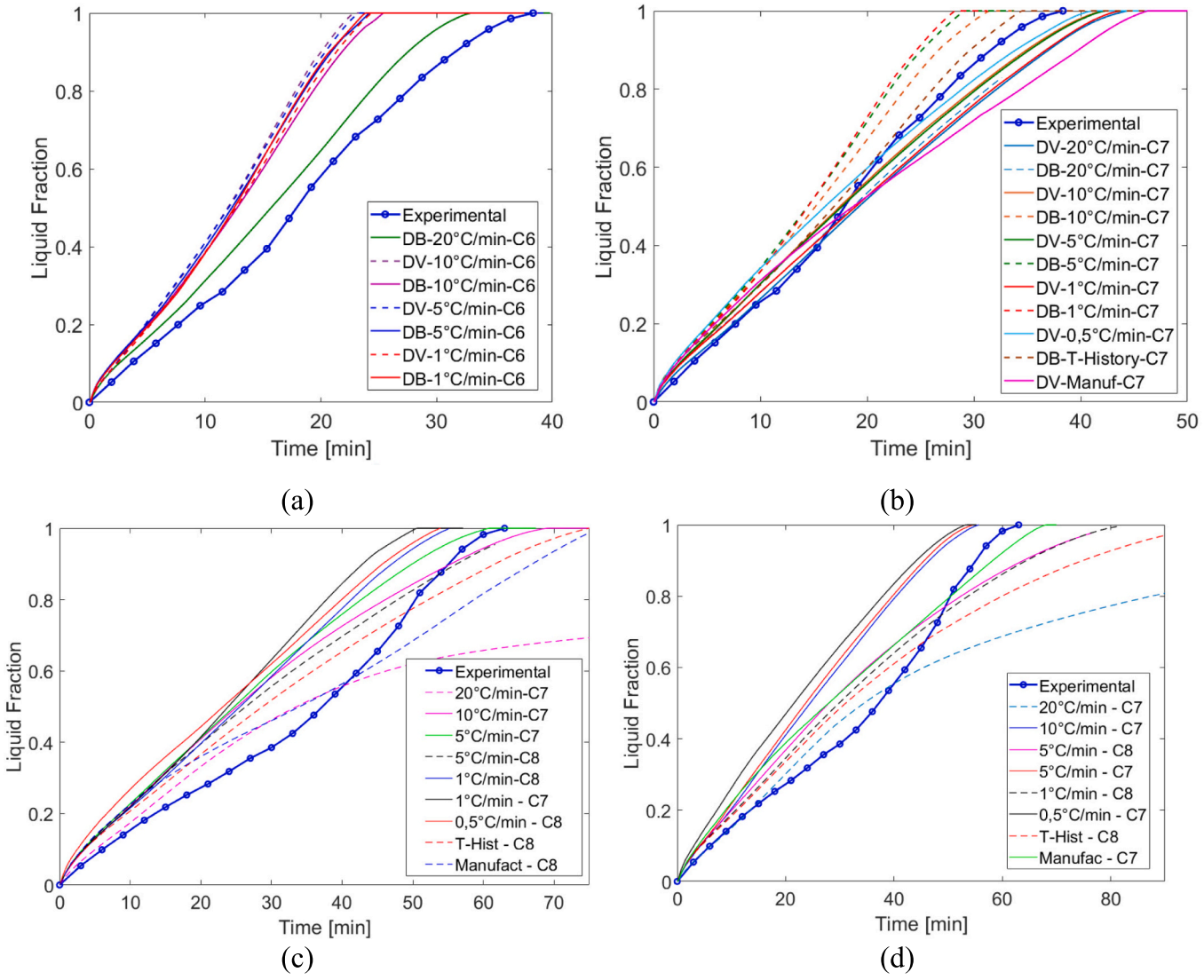

Fig. 12. Comparison of numerical and experimental results for liquid fraction (VD = variable density, BD = Boussinesq density), (a) ΔT = 10 °C and $C = 10^6$, (b) ΔT = 10 °C and $C = 10^7$, (c) ΔT = 5 °C and BD, (d) ΔT = 5 °C and VD.

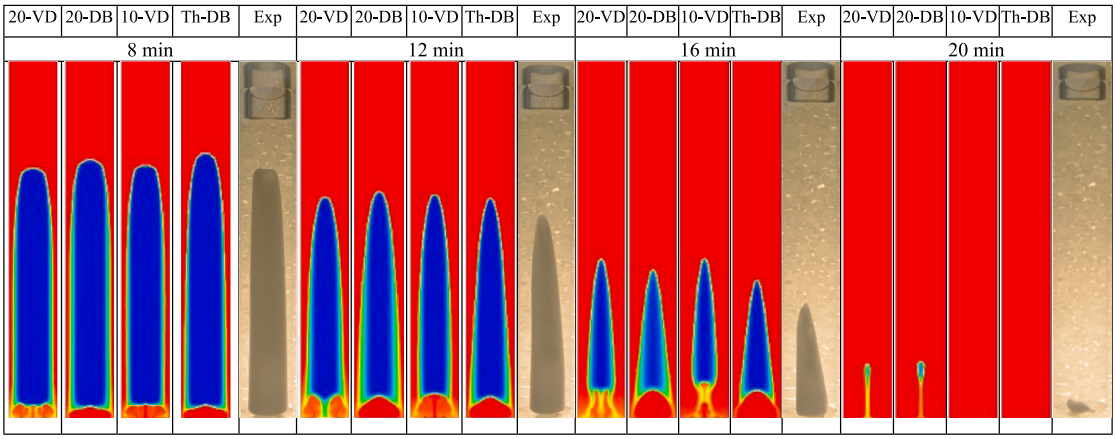

Fig. 13. Graphical evolution of the numerical molten fraction compared to experiment ($\Delta T = 15$ °C).

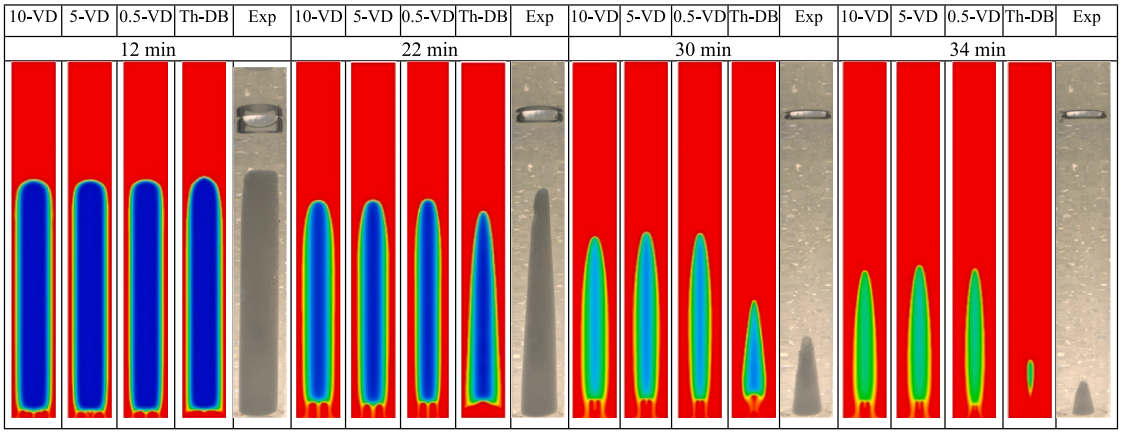

Fig. 14. Graphical evolution of the numerical molten fraction compared to experiment ($\Delta T = 10$ °C).

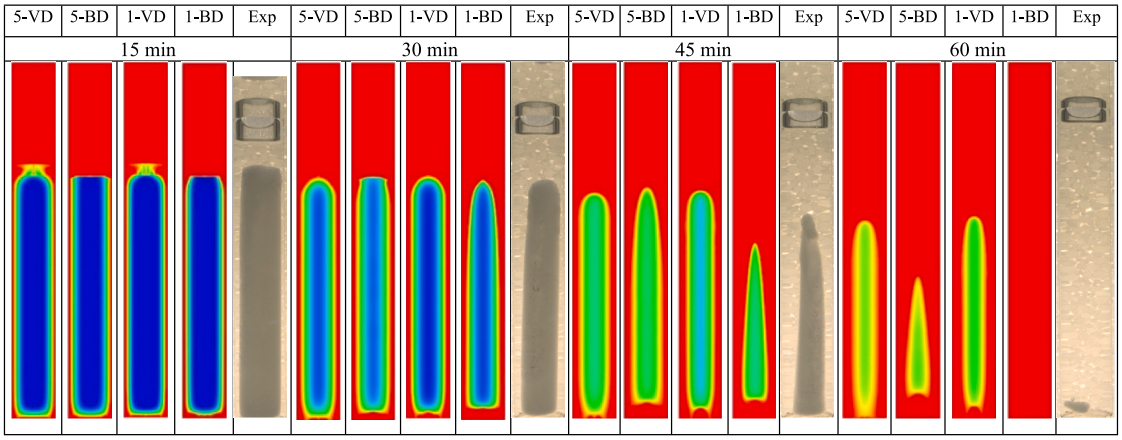

Fig. 15. Graphical evolution of the numerical molten fraction compared to experiment ($\Delta T = 5$ °C).

indicating that the practical limit of a pure material has been attained. In any case, as can be appreciated in Figs. 13-16, the dendritic region is restricted to less than one diameter height at the bottom of the test tube. Thus, the discrepancies seen, e.g., in Fig. 10, cannot be explained based solely on the artifact.

It is evident that the internal parameter C of the enthalpy-porosity model significantly influences the representation, and it is not clear how to choose a value that gives accurate results independently of other parameters. Also, the appearance of numerical artifacts is worst for larger ΔT (faster melting) and under the Boussinesq approximation, which indicates that it is linked to the modeling of the liquid formation and natural flow, in turn, influenced by the representation of phase change.

Finally, 3D patterns are observed, although, as seen in Figs. 13-15 and in accordance with previous literature [31], they are slight and don't justify a costly 3D numerical simulation.

During the numerical simulations, around 100 cases were evaluated varying the thermophysical properties of the material, considering a

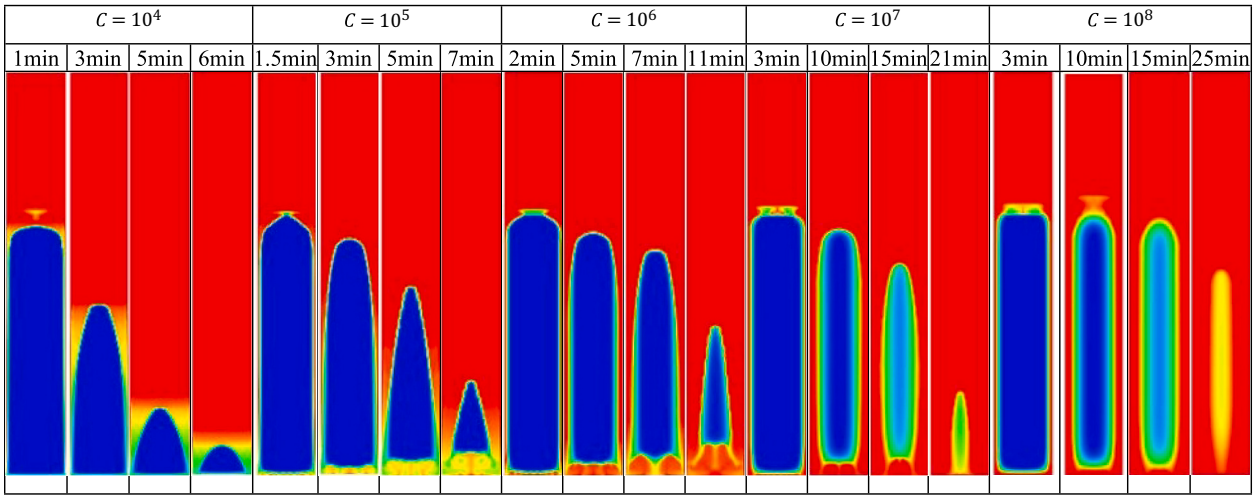

Fig. 16. Graphical evolution of the fusion contours varying the mushy zone constant.

variable or a constant density through the Boussinesq approximation. The boundary condition on the walls of the PCM container was varied by testing different ΔT. Different values of the constant of the mushy region were also tested. However, in none of the cases was it possible to achieve a generalization that is valid for all the results of the measurements.

4.3. Discussion

The results reveal that the constant of the mushy region in the enthalpy-porosity model affects the accuracy of the numerical simulation of the fusion of paraffin-type PCMs, and there are significant differences compared to experimental data when examining the melting patterns. No clear indications on how to choose the constant value for a given situation can be inferred from this study.

Future research directions and possible underlying effects could be as follows. It is worth noting that paraffins often exhibit multiple solid phases, which are observed in Figs. 1 and 2 and have been reported in the literature [50,51]. These transitions result from changes in molecular chain structure, geometry, and interactions, and involve low transition enthalpies, as appreciated in the figures. As a result, the curve representing a thermal magnitude during the solid-phase change exhibits a continuous variation of slope rather than a plateau as during fusion or solidification. This suggests a solid phase evolution before fusion occurs, and the enthalpy-porosity model cannot accurately represent it.

One possible alternative is to adjust the curve of effective specific heat versus temperature, which has been attempted previously but with limitations, only considering the main solid-liquid peak, and with the restriction of a merely diffusional problem also in the liquid. Also, DSC values depend on sample size and heat rate, requiring adjustment to the experiment or system being modeled. A combination of both methods may be a promising route, involving a universal variation of Cp representing all phases and an enthalpy-porosity technique that accounts for temperatures and latent heats from all transitions.

5. Conclusions

Numerical simulations of phase change in PCM materials are critical in investigating transient processes and systems. To achieve this, it is necessary to conduct an adequate thermal characterization of the materials' properties and their temperature dependence. This study aimed to investigate the impact of DSC-determined thermophysical properties of PCMs and inner, arbitrary parameters of enthalpy-porosity models on numerical simulations of phase change. The scenarios were evaluated using both the Boussinesq approximation and density variation with temperature. Additionally, the constant for the mushy zone was varied to compare melting curves in contexts closer to the beginning and end of the phase change. The obtained results were compared with experimental measurements, where the temperature of the thermal bath was varied between different experiments.

The main conclusions are:

- The results indicate that the enthalpy-porosity model is highly case-dependent when studying the PCMs considered in this work. Despite the exhaustive simulation campaign and characterization of thermophysical properties, with consideration of their temperature dependence, inconsistencies are evident in the model's ability to represent the physical phenomena observed experimentally in the various scenarios considered.
- It was found that the mushy zone constant of the porosity-enthalpy model is a major influence and cannot be universally adjusted to make numerical predictions agree with measurements. In particular, not only fusion times, but also the solidification patterns and liquid fraction time graphs exhibit notable, non-reducible disagreement. It seems not to be a simple and universal rationale to recommend a value of this constant applicable to a particular operating condition.
- Consequently, the enthalpy-porosity model for phase change of paraffine PCMs must be carefully considered in basic and applied studies.
- It is suggested tentatively that those difficulties may be due to the existence of multiple solid phases of the paraffin wax. This phenomenon is well documented and is not represented by the enthalpy-porosity model.
- Future developments may be tentatively based on alternative methods, such as representing the effective specific heat–temperature relationship, as determined by DSC, a multiple-phase enthalpy method, or a combination. All of them will demand, in any case, further adjustment and development.

Nomenclature

C	mushy zone constant, kg/m^3
c_p	specific heat, J/kg K
c_{eff}	effective heat capacity, J/kg K
D	tube diameter, cm
g	gravitational acceleration, m/s^2
p	pressure (Pa)
L	latent heat of fusion, kJ/kg
k	thermal conductivity, W/m-K
S	source term in equation of momentum

T	temperature, °C
t	time
W_h	immersion height, m

Greek symbols

μ	viscosity, kg/m-s
ρ	density, kg/m^3
γ	melt fraction
ΔT	temperature difference, °C

Subscripts

l	liquid
m	melting
s	solid

Credit authorship contribution statement

Arnold Martínez: Conceptualization, Data curation, Formal analysis, Funding acquisition, Investigation, Methodology, Project administration, Resources, Software, Supervision, Validation, Visualization, Writing – original draft, Writing – review & editing. **Mauricio Carmona:** Conceptualization, Data curation, Formal analysis, Funding acquisition, Investigation, Methodology, Project administration, Resources, Software, Supervision, Validation, Visualization, Writing – original draft, Writing – review & editing. **Cristóbal Cortés:** Conceptualization, Data curation, Formal analysis, Funding acquisition, Investigation, Methodology, Project administration, Resources, Software, Supervision, Validation, Visualization, Writing – original draft, Writing – review & editing. **Inmaculada Arauzo:** Conceptualization, Data curation, Formal analysis, Funding acquisition, Investigation, Methodology, Project administration, Resources, Software, Supervision, Validation, Visualization, Writing – original draft, Writing – review & editing.

Declaration of competing interest

The authors declare that they have no known competing financial interests or personal relationships that could have appeared to influence the work reported in this paper.

Data availability

No data was used for the research described in the article.

Acknowledgment

This study was made thanks to the help of the Ph.D. Scholarship Contract Identification Number: UN-OJ-2013-22063 of Universidad del Norte, the Scholarship Call No 727 of 2015 of COLCIENCIAS, and the program “Es tiempo de volver” of COLCIENCIAS.

References

[1] S. Zheng, et al., Assessment of the global energy transition: based on trade embodied energy analysis, Energy 273 (2023), 127274 jun. https://doi.org/10.1016/j.energy.2023.127274. jun.
[2] S. Gschwander, A. Lazaro, L.F. Cabeza, E. Günther, M. Fois, J. Chui, Development of a Test Standard for PCM and TCM Characterization Part 1: Characterization of Phase Change Materials, IEA Paris, France, 2011.
[3] A. D87-09, Standard Test Method for Melting Point of Petroleum Wax (Cooling Curve). Annual Book of Standards, ASTM International, West Conshocken, PA, 2018.
[4] A. D4419, Standard Test Method for Measurement of Transition Temperatures of Petroleum Waxes by Differential Scanning Calorimetry (DSC). Annual Book of Standards, ASTM International, West Conshohocken, PA, 2021.
[5] A. E793-06, Standard Test Method for Enthalpies of Fusion and Cristallization by Differential Scanning Calorimetry. Annual Book of Standards, ASTM International, West Conshohocken, PA, 2018.
[6] K. Wei, et al., Preparation of polyurethane solid-solid low temperature PCMs granular asphalt mixes and study of phase change temperature control behavior, Sol. Energy 231 (2022) 149–157, ene. https://doi.org/10.1016/j.solener.2021.11.056. ene.
[7] P. Du, et al., Anisotropic porous skeleton for efficient thermal energy storage and enhanced heat transfer: Experiments and numerical models, J. Energy Storage 56 (2022), 106021 dic. https://doi.org/10.1016/j.est.2022.106021.
[8] X. Li, H. Chen, L. Liu, Z. Lu, J.G. Sanjayan, W.H. Duan, Development of granular expanded perlite/paraffin phase change material composites and prevention of leakage, Sol. Energy 137 (2016) 179–188, nov. https://doi.org/10.1016/j.solener.2016.08.012. nov.
[9] O. Gencel, et al., Investigation of physico-mechanical, thermal properties and solar thermoregulation performance of shape-stable attapulgite based composite phase change material in foam concrete, Sol. Energy 236 (2022) 51–62, abr. https://doi.org/10.1016/j.solener.2022.02.042. abr.
[10] H. Mehling, P. Schossig, H.-P. Ebert, Development of standards for materials testing and quality control of PCM, in: 7th IIR Conference on Phase Change Materials and Slurries for Refrigeration and Air Conditioning, 2006.
[11] A. Lazaro, et al., Intercomparative tests on phase change materials characterisation with differential scanning calorimeter, Appl. Energy 109 (2013) 415–420, sep. https://doi.org/10.1016/j.apenergy.2012.11.045. sep.
[12] S. Gschwander, T. Haussmann, G. Hagelstein, C. Barreneche, G. Ferrer, L.F. Cabeza, Standarization of PCM characterization via DSC, in: Proceedings of SHC 2015 International Conference on Solar Heating and Cooling for Buildings and Industry, 2015, pp. 2–4.
[13] C. Barreneche, A.L. Pisello, A.I. Fernández, L.F. Cabeza, Experimental methods for the characterization of materials for latent thermal energy storage, in: A. Frazzica, L.F. Cabeza (Eds.), Recent Advancements in Materials and Systems for Thermal Energy Storage, Springer International Publishing, Cham, 2019, pp. 89–101, https://doi.org/10.1007/978-3-319-96640-3_7.
[14] X. Jin, X. Xu, X. Zhang, Y. Yin, Determination of the PCM melting temperature range using DSC, Thermochim. Acta 595 (2014) 17–21, nov. https://doi.org/10.1016/j.tca.2014.09.004. nov.
[15] Deutsches Institut Für Gütesicherung Und Kennzeichnung E.V, Phase Change Materials Quality Assurance RAL-GZ 896 [En línea]. Disponible en: https://www.pcm-ral.org/pdf/RAL_GZ_896_Phase_Change_Material_Edition_March_2018.pdf, 2018.
[16] H. Mehling, C. Barreneche, A. Solé, L.F. Cabeza, The connection between the heat storage capability of PCM as a material property and their performance in real scale applications, J. Energy Storage 13 (2017) 35–39, oct. https://doi.org/10.1016/j.est.2017.06.007. oct.
[17] L.F. Cabeza, et al., Unconventional experimental technologies available for phase change materials (PCM) characterization. Part 1. Thermophysical properties, Renew. Sust. Energ. Rev. 43 (2015) 1399–1414, mar. https://doi.org/10.1016/j.rser.2014.07.191. mar.
[18] Z. Yinping, J. Yi, J. Yi, A simple method, the -history method, of determining the heat of fusion, specific heat and thermal conductivity of phase-change materials, Meas. Sci. Technol. 10 (3) (1999) 201–205, mar. https://doi.org/10.1088/0957-0233/10/3/015. mar.
[19] J.M. Mar n, B. n Zalba, L.F. Cabeza, H. Mehling, Determination of enthalpy temperature curves of phase change materials with the temperature-history method: improvement to temperature dependent properties, Meas. Sci. Technol. 14 (2) (2003) 184–189, https://doi.org/10.1088/0957-0233/14/2/305.
[20] E. Günther, S. Hiebler, H. Mehling, R. Redlich, Enthalpy of phase change materials as a function of temperature: required accuracy and suitable measurement methods, Int. J. Thermophys. 30 (4) (2009) 1257–1269, https://doi.org/10.1007/s10765-009-0641-z.
[21] E.D. Kravvaritis, K.A. Antonopoulos, C. Tzivanidis, Improvements to the measurement of the thermal properties of phase change materials, Meas. Sci. Technol. 21 (4) (2010), 045103, https://doi.org/10.1088/0957-0233/21/4/045103.
[22] A. Solé, L. Miró, C. Barreneche, I. Martorell, L.F. Cabeza, Review of the T-history method to determine thermophysical properties of phase change materials (PCM), Renew. Sust. Energ. Rev. 26 (2013) 425–436, https://doi.org/10.1016/j.rser.2013.05.066.
[23] A. Hasan, S.J. McCormack, M.J. Huang, B. Norton, Characterization of phase change materials for thermal control of photovoltaics using differential scanning calorimetry and temperature history method, Energy Convers. Manag. 81 (2014) 322–329, https://doi.org/10.1016/j.enconman.2014.02.042.
[24] S. Liu, Y. Li, Y. Zhang, Review on heat transfer mechanisms and characteristics in encapsulated PCMs, Heat Transf. Eng. 36 (10) (2015) 880–901, https://doi.org/10.1080/01457632.2015.965093.
[25] E. Assis, L. Katsman, G. Ziskind, R. Letan, Numerical and experimental study of melting in a spherical shell, Int. J. Heat Mass Transf. 50 (9–10) (2007) 1790–1804, https://doi.org/10.1016/j.ijheatmasstransfer.2006.10.007.
[26] F.L. Tan, Constrained and unconstrained melting inside a sphere, Int. Commun. Heat Mass Transf. 35 (4) (2008) 466–475, https://doi.org/10.1016/j.icheatmasstransfer.2007.09.008.
[27] F.L. Tan, S.F. Hosseinizadeh, J.M. Khodadadi, L. Fan, Experimental and computational study of constrained melting of phase change materials (PCM) inside a spherical capsule, Int. J. Heat Mass Transf. 52 (15–16) (2009) 3464–3472, https://doi.org/10.1016/j.ijheatmasstransfer.2009.02.043.

[28] B.J. Jones, D. Sun, S. Krishnan, S.V. Garimella, Experimental and numerical study of melting in a cylinder, Int. J. Heat Mass Transf. 49 (15–16) (2006) 2724–2738, https://doi.org/10.1016/j.ijheatmasstransfer.2006.01.006.
[29] H. Shmueli, G. Ziskind, R. Letan, Melting in a vertical cylindrical tube: numerical investigation and comparison with experiments, Int. J. Heat Mass Transf. 53 (19–20) (2010) 4082–4091, sep. https://doi.org/10.1016/j.ijheatmasstransfer.2010.05.028. sep.
[30] P.A. Galione, O. Lehmkuhl, J. Rigola, A. Oliva, Fixed-grid numerical modeling of melting and solidification using variable thermo-physical properties – application to the melting of n-Octadecane inside a spherical capsule, Int. J. Heat Mass Transf. 86 (2015) 721–743, https://doi.org/10.1016/j.ijheatmasstransfer.2015.03.033.
[31] M.G. Broadhurst, An analysis of the solid phase behavior pf the normal paraffins, J. Res. Natl. Bur. Stand. Sect. A 66A (3) (1962) 241–249.
[32] O. Younis, et al., Numerical investigation of thermal energy storage system loaded with nano-enhanced phase change material with Koch snowflake fractal cross-section, J. Energy Storage 56 (2022), 106016, https://doi.org/10.1016/j.est.2022.106016.
[33] X. Zuo, X. Zhao, J. Li, Y. Hu, H. Yang, D. Chen, Enhanced thermal conductivity of form-stable composite phase-change materials with graphite hybridizing expanded perlite/paraffin, Sol. Energy 209 (2020) 85–95, https://doi.org/10.1016/j.solener.2020.08.082.
[34] C. Liu, C. Luo, T. Xu, P. Lv, Z. Rao, Experimental study on the thermal performance of capric acid-myristyl alcohol/expanded perlite composite phase change materials for thermal energy storage, Sol. Energy 191 (2019) 585–595, https://doi.org/10.1016/j.solener.2019.09.049.
[35] M.M. Kenisarin, K. Mahkamov, S.C. Costa, I. Makhkamova, Melting and solidification of PCMs inside a spherical capsule: a critical review, J. Energy Storage 27 (2020), 101082, https://doi.org/10.1016/j.est.2019.101082.
[36] M. Faden, A. König-Haagen, E. Franquet, D. Brüggemann, Influence of density change during melting inside a cavity: theoretical scaling laws and numerical analysis, Int. J. Heat Mass Transf. 173 (2021), 121260, https://doi.org/10.1016/j.ijheatmasstransfer.2021.121260.
[37] M. Iten, S. Liu, A. Shukla, P.D. Silva, Investigating the impact of C p -T values determined by DSC on the PCM-CFD model, Appl. Therm. Eng. 117 (2017) 65–75, https://doi.org/10.1016/j.applthermaleng.2017.02.021.
[38] A. Buonomano, F. Guarino, The impact of thermophysical properties and hysteresis effects on the energy performance simulation of PCM wallboards: experimental studies, modelling, and validation, Renew. Sust. Energ. Rev. 126 (2020), 109807, https://doi.org/10.1016/j.rser.2020.109807.
[39] M. Barthwal, D. Rakshit, No fins attached? Numerical analysis of internal–external fins coupled PCM melting for solar applications, Appl. Therm. Eng. 215 (2022), 118911 oct. https://doi.org/10.1016/j.applthermaleng.2022.118911. oct.
[40] S. Rana, M. Zunaid, R. Kumar, CFD analysis for heat transfer comparison in circular, rectangular and elliptical tube heat exchangers filled with PCM, Mater. Today: Proc. 56 (2022) 637–644, https://doi.org/10.1016/j.matpr.2021.12.412.
[41] M. Mozafari, K. Hooman, A. Lee, S. Cheng, Numerical study of a dual-PCM thermal energy storage unit with an optimized low-volume fin structure, Appl. Therm. Eng. 215 (2022), 119026 oct. https://doi.org/10.1016/j.applthermaleng.2022.119026. oct.
[42] FLUENT, ANSYS. R2 User's Manual, ANSYS. INC, Canonsburg, PA, USA, 2020.
[43] C. Castellón, E. Günther, H. Mehling, S. Hiebler, L.F. Cabeza, Determination of the enthalpy of PCM as a function of temperature using a heat-flux DSC-A study of different measurement procedures and their accuracy, Int. J. Energy Res. 32 (13) (2008) 1258–1265, https://doi.org/10.1002/er.1443.
[44] A. Martínez, M. Carmona, C. Cortés, I. Arauzo, Characterization of thermophysical properties of phase change materials using unconventional experimental technologies, Energies 13 (18) (2020) 4687, https://doi.org/10.3390/en13184687.
[45] ASTM E1269-9, Test Method for Determining Specific Heat Capacity by Differential Scanning Calorimetry, ASTM International, West Conshohocken, PA, 2018, https://doi.org/10.1520/E1269-11R18.
[46] ANSYS, ANSYS Fluent Theory Guide R2, 2020.
[47] A.D. Brent, V.R. Voller, K.J. Reid, Enthalpy-porosity technique for modeling convection-diffusion phase change: application to the melting of a pure metal, Numer. Heat Transf. 13 (3) (1988) 297–318, https://doi.org/10.1080/10407788808913615.
[48] V.R. Voller, C. Prakash, A fixed grid numerical modelling methodology for convection-diffusion mushy region phase-change problems, Int. J. Heat Mass Transf. 30 (8) (1987) 1709–1719, https://doi.org/10.1016/0017-9310(87)90317-6.
[49] N. Mallya, S. Haussener, Buoyancy-driven melting and solidification heat transfer analysis in encapsulated phase change materials, Int. J. Heat Mass Transf. 164 (2021), 120525, https://doi.org/10.1016/j.ijheatmasstransfer.2020.120525.
[50] H. Fröhlich, Phase transitions of solid paraffins and the flexibility of hydrocarbon chains, Trans. Faraday Soc. 40 (0) (1944) 498–502, https://doi.org/10.1039/TF9444000498.
[51] P.K. Sullivan, Solid-phase behavior of several long-chain n-paraffins, esters, and a ketone, J. Res. Natl. Bur. Stand. Sect. A: Phys. Chem. 78A (2) (1974) 129, https://doi.org/10.6028/jres.078A.009.